Available online at www.sciencedirect.com
ScienceDirect
Applied Catalysis B: Environmental 82 (2008) 199–207
APPLIED CATALYSIS B: ENVIRONMENTAL
www.elsevier.com/locate/apcatb

New sulfur adsorbents derived from layered double hydroxides II. DRIFTS study of COS and H_2S adsorption

Todd J. Toops [a,*], Mark Crocker [b]

[a] *Fuels, Engines and Emissions Research Center, Oak Ridge National Laboratory, 2360 Cherahala Boulevard, Knoxville, TN 37932-1563, United States*
[b] *Center for Applied Energy Research, University of Kentucky, 2540 Research Park Drive, Lexington, KY 40511-8479, United States*

Received 22 August 2007; received in revised form 9 November 2007; accepted 15 January 2008
Available online 20 January 2008

Abstract

H_2S and COS adsorption were studied on two calcined layered double hydroxides (LDHs), $Mg_{0.75}Al_{0.25}(OH)_2(CO_3)_{0.125}$ and $Mg_{0.65}Al_{0.35}(OH)_2(CO_3)_{0.175}$, using diffuse reflectance infrared Fourier transform spectroscopy (DRIFTS) and a chemisorption apparatus. Both demonstrated the ability to irreversibly adsorb H_2S, corresponding to uptakes of 1.54 and 1.76 μmol/m^2, respectively, but $Mg_{0.75}Al_{0.25}$ had a significantly larger capacity for COS, 1.62 μmol/m^2 compared to 0.80 μmol/m^2 for $Mg_{0.65}Al_{0.35}$. Analysis of the DRIFT spectra suggests the adsorption of H_2S proceeds via the substitution of lattice oxygen with sulfur, resulting in the formation of H_2O on the surface. COS adsorption is more complicated, although it appears that a similar substitution of lattice oxygen with sulfur occurs. This results in the formation of CO_2 and subsequently bicarbonates and carbonates. The formation of hydrogen thiocarbonate is also involved, although this form is generally only observed in the later stages of adsorption and appears to form at the expense of bicarbonate. The $Mg_{0.75}Al_{0.25}$ LDH retained its ability to adsorb COS in the presence of propene.

Keywords: DRIFTS; Adsorption; Carbonyl sulfide; Layered double hydroxide; Hydrotalcite

1. Introduction

Energy efficiency in transportation and power generation can help to conserve fossil fuel resources, as well as lessen the amount of CO_2 emitted to the atmosphere. A major barrier to the implementation of energy efficient technologies, however, is the presence of fuel-borne sulfur. Sulfur is a ubiquitous poison, which in both its oxidized and reduced forms (e.g., SO_2, SO_3; H_2S, COS) can act as a catalyst poison due to its ability to adsorb strongly onto metal and metal oxide surfaces.

Fuel cells represent a particularly promising technology for clean and efficient power generation. In order to facilitate the use of coal-derived syngas or hydrocarbon fuels as feedstocks for fuel cells, the sulfur content of the feed must be reduced to very low levels. In the case of proton-exchange membrane (PEM) fuel cells, it is necessary to set the allowable sulfur concentration at levels as low as 10 ppb in order to maximize system durability [1]. Typically sulfur in these feedstocks is present as H_2S and to a lesser extent COS. Traces of mercaptans (RSH) can also be present. Removal of these compounds is necessitated by the poisoning effect that sulfur compounds exert on both water-gas shift catalysts (for syngas processing) and the platinum catalyst in the fuel cell electrodes.

In the case of a hydrocarbon fuel, direct removal of the sulfur compounds using a regenerable adsorbent is an attractive means of achieving the low sulfur level required. In the case of coal-derived syngas, the high initial sulfur level (typically around 1% H_2S) requires a multi-step treating process, such as the use of an amine absorbent, followed by a polishing step. In principle, use of a solid adsorbent is an attractive option for this latter step. Unfortunately, commercial sulfur adsorbents are generally not able to achieve the very high removal efficiencies required at ambient temperature. For this reason new adsorbents are required, which combine high sorption capacity with an improved temperature range of operation.

Layered double hydroxides (LDHs) are lamellar mixed metal hydroxides and are readily synthesized via co-precipitation methods. The structure of these compounds consists of

* Corresponding author. Tel.: +1 865 946 1207; fax: +1 865 946 1354.
E-mail address: toopstj@ornl.gov (T.J. Toops).

0926-3373/$ – see front matter © 2008 Elsevier B.V. All rights reserved.
doi:10.1016/j.apcatb.2008.01.013

positively charged layers owing to the presence of two metal hydroxides in different oxidation states. The necessary charge balance is maintained by anions located in the interlayer region. In general, these compounds can be formulated as $[M_{1-x}^{2+}M_x^{3+}(OH)_2]A_{x/n}^{n-}\cdot mH_2O$, the mineral hydrotalcite, $[Mg_{0.75}Al_{0.25}(OH)_2](CO_3)_{0.125}\cdot 0.5H_2O$, being the most prominent member of this group [2]. Within the context of sulfur adsorption, LDHs are of interest due to their basicity and high surface area, which renders them excellent adsorbents for acidic species. Indeed there are literature reports of CO_2 and SO_x adsorption by layered double hydroxides [3–9], while recent work has shown them to be active for COS adsorption at room temperature [10].

Further, synthetic studies have shown that LDHs possess great flexibility with respect to the degree in which their chemical and physical properties can be modified. This suggests that it should be possible to tune the properties of an LDH adsorbent so as to optimize its performance for the sorption of a given sulfur compound. However, to meet this goal, an understanding of the mechanism of adsorption is desirable. In this context, we have applied diffuse reflectance infrared Fourier transform spectroscopy (DRIFTS) to study COS and H_2S adsorption on calcined hydrotalcite.

2. Experimental

Two LDH samples were used in this work, $Mg_{0.75}Al_{0.25}(OH)_2(CO_3)_{0.125}$ and $Mg_{0.65}Al_{0.35}(OH)_2(CO_3)_{0.175}$, which hereafter are respectively abbreviated as $Mg_{0.75}Al_{0.25}$ and $Mg_{0.65}Al_{0.35}$. Samples were prepared according to the method of Reichle [11]. A solution of $Mg(NO_3)_2\cdot 6H_2O$ and $Al(NO_3)_3\cdot 9H_2O$ (0.4 mol total metals) in 210 ml deionized water was added dropwise at room temperature to 330 ml of an aqueous solution containing Na_2CO_3 (30 g, 0.28 mol) and the calculated amount of NaOH required to react with the M^{2+} and M^{3+} ions. Vigorous stirring was maintained throughout the ~60 min addition period. The resulting precipitate was left to age in the reaction mixture under gentle stirring at 75 °C overnight and was subsequently isolated by a cycle of centrifuging/decanting/washing with deionized water until the washings attained a pH of 7. The resulting solid was dried at 60 °C in a vacuum oven. The measured residual sodium content was in both cases <500 ppm. Powder X-ray diffractograms (not shown) confirmed that the LDH was the only crystalline phase present in each product.

The characterization of the LDH adsorption behavior and chemistry was performed using two capabilities. The first was a diffuse reflectance infrared Fourier transform spectroscopy (DRIFTS) instrument which employs a high temperature gas cell. The second was a chemisorption/physisorption gas cell which was used to measure specific surface area and quantify the LDH sulfur adsorption capacity. Each system was fully equipped for gas flow and heat treatments.

Before experimentation in either system the samples were heated to 450 °C in N_2 (99.999% pure) flowing at 50 cm^3 (STP) per minute (sccm). To monitor the impact of the thermal activation on the LDH, N_2 physisorption measurements were performed in the adsorption cell according to the BET method. The cell, described in full detail elsewhere [12], consists of a pyrex manifold for introducing gases, a U-shaped quartz sample cell, and a high-vacuum system that provides base pressures in the low 10^{-7} Torr range when evacuating the manifold. The system was configured to allow gas flow through the sample cell using mass flow controllers. All o-rings in the Pyrex/stainless steel system were made of perfluoroelastomers. The sample cell was heated with a vertical furnace in conjunction with a PID temperature controller. Isotherm pressure readings were obtained using a pressure transducer with 0.01% full-scale accuracy. Fresh samples were pretreated overnight at 450 °C, evacuated to the base pressure, and then cooled. Once thermal stability was achieved in the sample cell, the probe gas was introduced. The pure gas, either H_2S (99.5%) or COS (99.5%), was then allowed to equilibrate with the surface at pressures between 50 and 250 Torr. This was repeated to record several data points and a linear relationship between molar uptake and pressure was achieved. The reversible uptake was then measured by evacuating to the base pressure for 1 h and repeating the procedure.

The DRIFTS system has been fully detailed in earlier papers [12,13]. It consists of a *MIDAC* model M2500 FTIR spectrometer coupled to a *Harrick Scientific* barrel ellipsoidal mirror DRIFT accessory with an integrated stainless-steel reaction cell. This barrel-ellipse DRIFTS accessory is designed to maximize the collection of the diffusely scattered infrared beam; nearly 360° of the reflected beam is collected. The LDH materials were observed under carefully controlled temperature and gas-flow conditions. The system can be heated to 525 °C and is typically operated at slightly below atmospheric pressure, ca. 500 Torr, to prevent stagnation in the cell and to maintain the seal between the removable hemispherical ZnSe dome and the cell body. Mass flow controllers establish the inlet gas concentrations. The reactant gases used in the measurements had the following concentrations and purities: 5% COS (99.5%) in Ar, 10% H_2S (99.5%) in Ar, and 20% propene (99+%) in Ar. All argon balance gases were ultra high purity (99.999%).

Before exposure to the sulfur containing gas mixtures, each sample was pretreated in the DRIFTS reactor cell by heating to 450 °C and reacting with a 50 sccm flow of 1% H_2/N_2. The pretreatment was continued overnight to ensure complete transformation of the LDH into the mixed oxide. Following pretreatment, the N_2 flow was continued while the sample was cooled to room temperature. While cooling from 450 °C to room temperature, a DRIFT spectrum of the pretreated sample was recorded every 50 °C. Once at room temperature, the cell was sealed under N_2, and the sulfur-containing gas mixture was routed through the bypass loop for 5 min to stabilize the gas mixture concentrations. For each flow condition, the sample was allowed to saturate in the sulfur-containing mixture, usually overnight. In some instances, the samples were heated to 450 °C following saturation. Spectra were collected every 50 °C and compared to the files recorded during the initial cooling period.

Each DRIFT spectrum is converted to absorbance units using a background spectrum that is acquired with a brushed

Table 1
LDH properties

LDH	Surface area (m^2/g)		H_2S uptake (μmol/m^2) (wt% S)		COS uptake (μmol/m^2) (wt% S)	
	Initial	Treated	Total	Irreversible	Total	Irreversible
$Mg_{0.75}Al_{0.25}$	73.7	211	2.79 (1.89)	1.54 (1.04)	2.25 (1.52)	1.62 (1.10)
$Mg_{0.65}Al_{0.35}$	68.6	254	3.07 (2.50)	1.76 (1.43)	1.48 (1.21)	0.80 (0.65)

BET surface area measured with N_2; H_2S and COS capacity measured with static chemisorption.

aluminum plate. This file was used to convert the reflectance files into absorbance units using:

$$\text{Absorbance} = -\log_{10}\left[\frac{\text{sample file}}{\text{background file}}\right] \quad (1)$$

Both sample and background files are temperature dependent, so a background file is recorded at each temperature of interest. Once reflectance spectra have been converted into absorbance units the spectra can be compared and even subtracted from each other for a given temperature.

3. Results

3.1. LDH pretreatment

Thermal pretreatment of the LDHs results in both surface area changes and spectroscopic transformations. As shown in Table 1, upon pretreatment the measured BET surface area increases from 73.7 to 211 m^2/g for $Mg_{0.75}Al_{0.25}$ and from 68.6 to 254 m^2/g for $Mg_{0.65}Al_{0.35}$. This increase in surface area upon LDH calcination has been attributed to the formation of micro- and mesopores due to expulsion of CO_2 and H_2O from the LDH [14,15], although in this work we did not observe micropore formation. Fig. 1a and b shows the DRIFT spectra of $Mg_{0.75}Al_{0.25}$ and $Mg_{0.65}Al_{0.35}$ while heating from room temperature to 450 °C. To enable a direct comparison between the initial surface and pretreated surface, spectra were also recorded after cooling to room temperature. The spectral changes are similar for both samples, and after the pretreatment the spectra are nearly identical with peaks at 1534, 1412, and 1080 cm^{-1} for $Mg_{0.75}Al_{0.25}$ and 1533, 1418, and a broad peak covering 1080–1020 cm^{-1} for $Mg_{0.65}Al_{0.35}$. These features are indicative of the presence of monodentate carbonate, the specific vibrations being listed in Table 2 for $Mg_{0.75}Al_{0.25}$.

3.2. COS and H_2S chemisorption

For the purposes of the DRIFTS measurements, it was decided to choose the sample with the best sulfur adsorption capacity. This was determined with static chemisorption measurements using pure H_2S and COS. The isotherms for both samples are displayed in Fig. 2a for H_2S and Fig. 2b for COS. The total uptake was measured for each gas, followed by evacuation for 1 h, and then the reversible uptake was measured. To determine the total and reversible uptakes, the linear isotherms are extrapolated to 225 ppm, i.e. 0.17 Torr, and

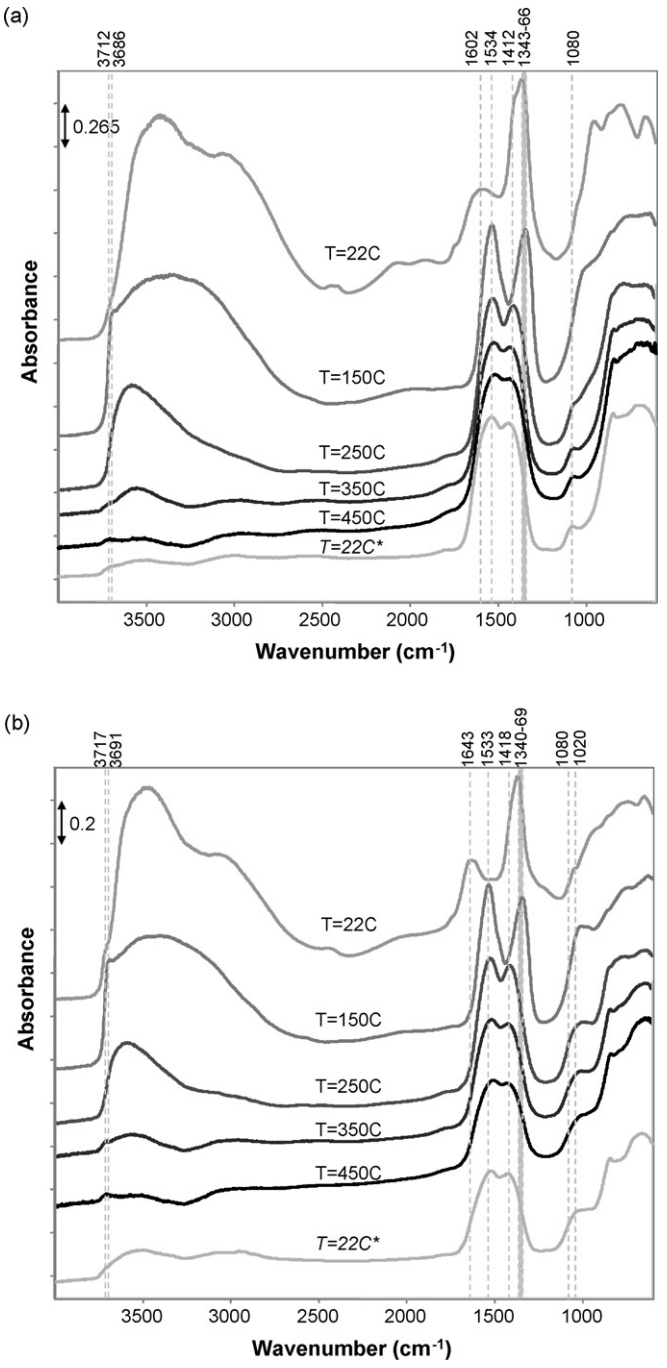

Fig. 1. Effect of thermal pretreatment on (a) $Mg_{0.75}Al_{0.25}$ and (b) $Mg_{0.65}Al_{0.35}$, while heating in N_2 from room temperature to 450 °C and then back to room temperature. The background spectrum was a blank brushed aluminum plate recorded at each temperature.

Table 2
DRIFTS peak assignments based on this study for adsorbates on $Mg_{0.75}Al_{0.25}$

Hydrogen thiocarbonate		Dithiocarbonate		Bicarbonate		Monodentate carbonate		Bidentate carbonate	
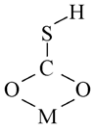		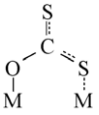		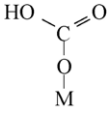		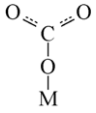		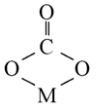	
Wavenumber (cm^{-1})	Bond	Wavenumber (cm^{-1})	Bond	Wavenumber (cm^{-1})	Bond	Wavenumber (cm^{-1})	Bond	Wavenumber (cm^{-1})	Bond
$Mg_{0.75}Al_{0.25}$									
1602–11	–	1154–75	ν C–O	1645–86	ν C=O	1505–30	ν_{as} COO^-	1600–11	ν C=O
1370–90	–	1080–90	ν C–S	1405–14	ν_{as} COO^-	1408–14	ν_s COO^-	1260–65	ν_{as} COO^-
		1005–35	ν C–$S_{surface}$	1222–25	β OH	1080–90	ν C–O	1000–35	ν_s COO^-
				1080–90	ν_s COO^-				

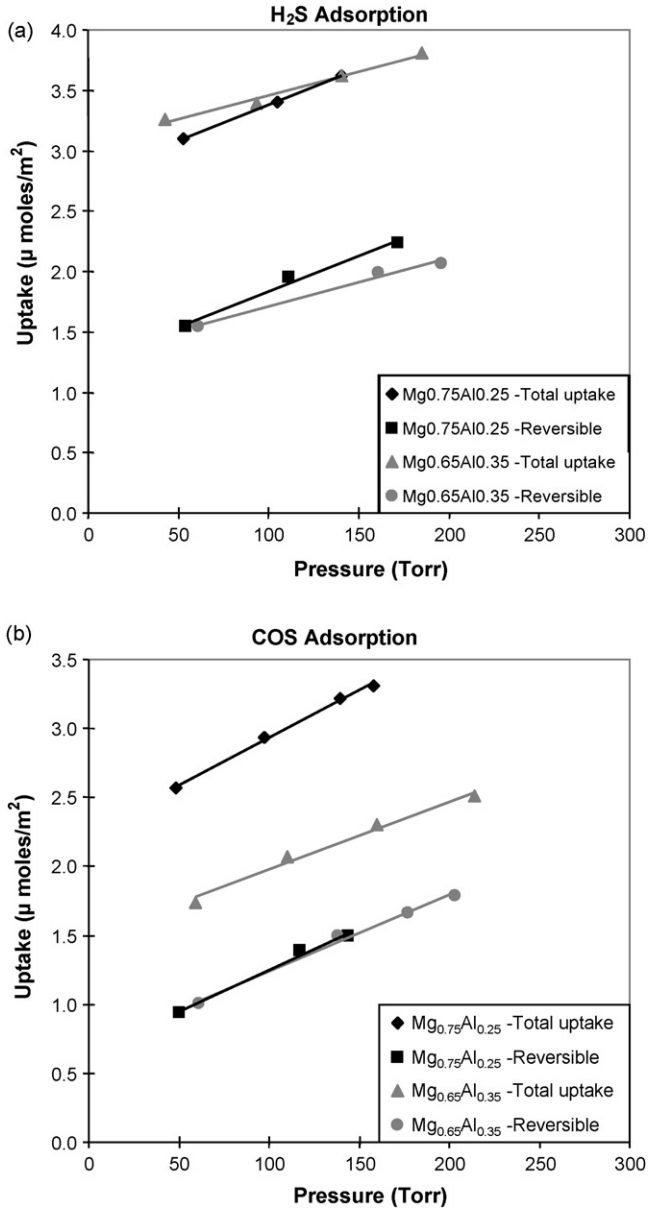

Fig. 2. Isotherms for (a) H_2S and (b) COS adsorption on $Mg_{0.75}Al_{0.25}$ and $Mg_{0.65}Al_{0.35}$. Static chemisorption measurements recorded at 22 °C using pure gases.

the difference in the two isotherms is taken to be the irreversible uptake. From Fig. 2, it follows that the total H_2S uptake was 2.79 and 3.07 μmol/m^2 for $Mg_{0.75}Al_{0.25}$ and $Mg_{0.65}Al_{0.35}$, respectively, and after accounting for the reversible uptake, the irreversible uptake was determined to be 1.54 and 1.76 μmol/m^2. Similarly for COS, the total uptake was 2.25 and 1.48 μmol/m^2 for $Mg_{0.75}Al_{0.25}$ and $Mg_{0.65}Al_{0.35}$, respectively, and the irreversible uptake was 1.62 and 0.80 μmol/m^2. These results are summarized in Table 1. While $Mg_{0.65}Al_{0.35}$ demonstrated 14% more H_2S capacity, it only had half of the COS capacity of $Mg_{0.75}Al_{0.25}$. Due to this significant difference in performance, $Mg_{0.75}Al_{0.25}$ was the focus of the DRIFTS study.

3.3. DRIFTS analysis of COS and H_2S adsorption

As indicated above, each sample was pretreated at 450 °C overnight and then cooled to room temperature. A background spectrum was recorded immediately upon the temperature reaching 22 °C, which was used as the baseline condition for the sulfur adsorption studies. At this point, the LDH was active for adsorption, and a reproducible surface had been achieved. Following adsorption the cell was purged in N_2 to remove any weakly adsorbed species and to simplify the spectra from gas-phase contributions. Fig. 3a shows the spectra obtained after adsorption of 1% H_2S flowing in 50 sccm of N_2 and is referenced to the initial condition such that all features shown in the figure are due to the interaction of $Mg_{0.75}Al_{0.25}$ with the gas phase. There are significant spectral changes in the first 10 min, as the hydroxyl region (3000–4000 cm^{-1}) undergoes significant growth and several features arise between 1000 and 2000 cm^{-1}. Within the first 10 min there is a large peak apparent at 1633 cm^{-1}, a minor one at 2577 cm^{-1}, and a negative peak at 3724 cm^{-1}; each of these increases modestly over the next 16 h if at all. The peak at 2577 cm^{-1} can be attributed to the H–S vibration, and since a doublet is not apparent it most likely indicates H_2S dissociative adsorption to form an M–SH species and a hydroxyl group [16,17].

As discussed in Section 4 below, among several possible routes for H_2S adsorption, reaction with surface hydroxyl groups can lead to the generation of molecularly adsorbed H_2O (1633 cm^{-1}). Molecularly adsorbed H_2O would contribute to

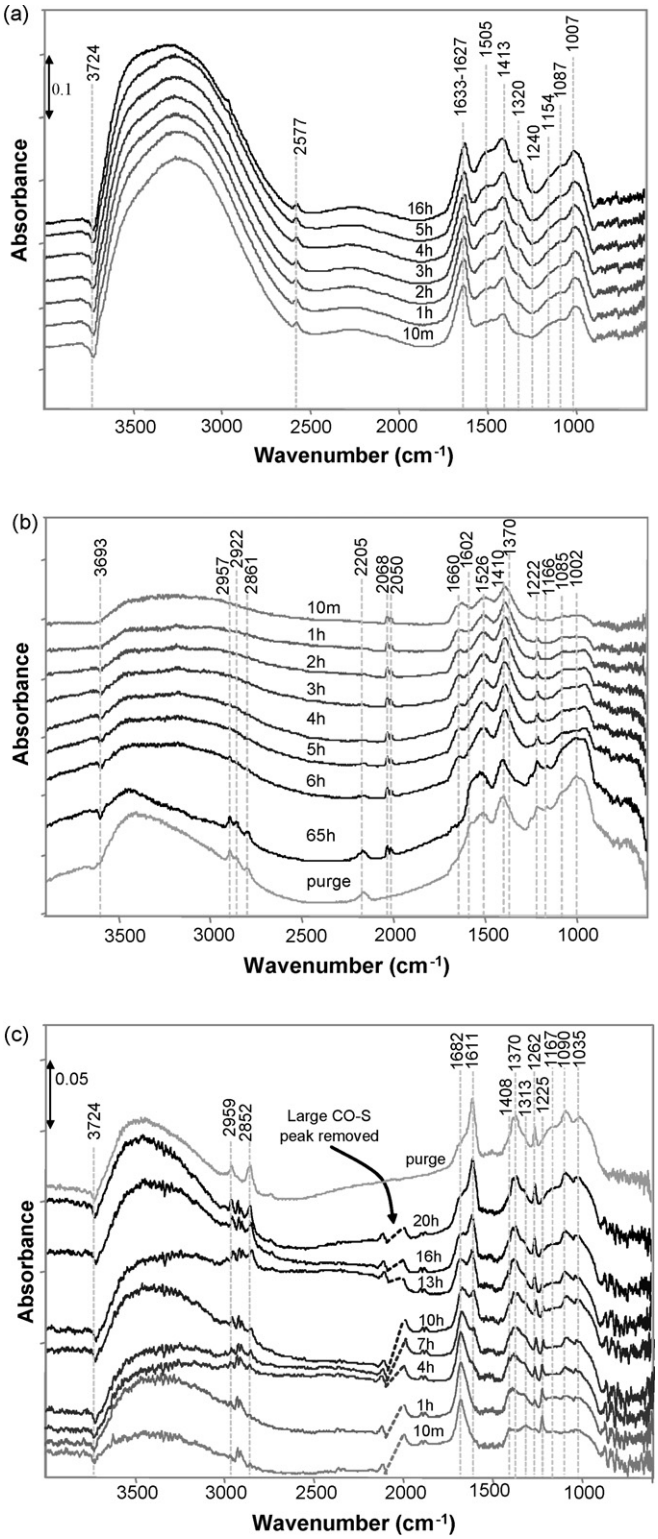

Fig. 3. Background-subtracted DRIFT spectra recorded at 22 °C of (a) 1% H_2S, (b) 225 ppm COS, and (c) 1% COS adsorption on $Mg_{0.75}Al_{0.25}$ at various times. The background spectrum was pretreated $Mg_{0.75}Al_{0.25}$ recorded just prior to introduction of the sulfur-containing stream.

the large hydroxyl features, and the negative peak at 3724 cm^{-1} can be attributed to the initial hydroxyl group that initiated the reaction. This results in the formation of S^{2-} groups on the oxide surface, which do not have a characteristic IR absorption frequency. Due to the relative stability of these peaks, this appears to be a kinetically fast step that is only limited by the availability of adsorption sites.

The peaks that have the most significant growth throughout the adsorption experiments are located at 1505, 1413, and 1320 cm^{-1}. The feature at 1320 cm^{-1} coincides with physisorbed SO_2, which could arise from the interaction of S^{2-} with trace levels of O_2 in the feed or perhaps even lattice oxygen. Based on the assignments given earlier it follows that the bands at 1505 and 1413 cm^{-1} correspond to monodentate carbonate, especially since there also appears to be a small amount of concurrent growth at 1087 cm^{-1}. Due to the length of this experiment this adsorption is most likely due to trace amounts of CO_2 in the feed. The IR bands reported in the literature for these various functional groups, as well as several other pertinent adsorbates, are listed in Table 3 for similar sulfur adsorbent materials [16,18–33].

Fig. 3b depicts the adsorption of 225 ppm COS on $Mg_{0.75}Al_{025}$ at 22 °C. The spectral features that are apparent within the first 10 min occur at 1660, 1526 and 1410 cm^{-1}, along with a sharp, albeit small, peak at 1222 cm^{-1}. The presence of these peaks suggests the simultaneous formation of bicarbonate (1660, 1410, 1222, and 1085 cm^{-1}) and monodentate carbonate (1526, 1410, and 1085 cm^{-1}). The lack of immediately identifiable sulfur species suggests that, similar to H_2S formation, COS is reacting with the surface to form S^{2-}. After flowing the sulfur stream for 65 h there are small but significant changes in the spectra. The peak at 1660 cm^{-1} is no longer significant, but instead there is a band at 1602 cm^{-1} and there is some evidence of a shoulder near 1370 cm^{-1}. These two peaks are proposed to correspond to hydrogen-thiocarbonate (HTC), and the spectra suggest that the bicarbonate is being converted to the sulfur containing HTC after several hours on stream. There is also substantial growth in the peaks near 1000 cm^{-1}. There are many contributions at the lower wavenumbers, with one possibility being the formation of dithiocarbonate, DTC (1166, 1085, and 1002 cm^{-1}); SO_3^{2-} and HSO_3^- formation are also possibilities. Also observed at long reaction times, are peaks located just below 3000 cm^{-1} which correspond to saturated alkanes. These can attributed to the presence of trace amounts of impurities in the gas feed, probably mercaptans. The feature at 2205 cm^{-1} has not been identified and is not reproducible; it appears to be an artifact.

Fig. 3c shows the adsorption of 1% COS at 22 °C. Prominent peaks at 1682, 1262, and 1225 cm^{-1} and broad peaks at 1408, 1313, 1090 and 1035 cm^{-1} are apparent within the first hour of adsorption. Similar to the adsorption of 225 ppm COS (Fig. 3b), these peaks suggest that bicarbonate initially forms (1682, 1408, 1225, and 1090 cm^{-1}), and the lack of identifiable sulfur species at the outset continues to suggest that COS is reacting to form S^{2-}. Unlike adsorption at the lower COS concentration, there is no evidence of monodentate carbonate formation since there are no peaks apparent between 1500 and 1600 cm^{-1}; however, the presence of peaks at 1611, 1262 and 1035 cm^{-1}, which start growing in after 1 h, suggest that bidentate carbonate is forming. After 4 h of adsorption, there is evidence of HTC formation (peaks at 1611 and 1370 cm^{-1}). The IR

Table 3
Reported IR bands for adsorbates of interest on metal oxides

Wavenumber (cm^{-1})	Functional group	Vibration	Reference
Al_2O_3			
1313–1360, 1546–1578	H-thiocarbonate	–	[18–25,28]
1151–1183	Dithiocarbonate	ν C–O	[21]
1045–1080	Dithiocarbonate	ν C–S	[21]
1009–1032	Dithiocarbonate	ν C–$S_{surface}$	[21]
1648–1659	Bicarbonate	ν C=O	[18,22]
1430–1440	Bicarbonate	ν_{as} COO^-	[18,22]
1230	Bicarbonate	β OH	[18,22]
1470–1530	Monodentate carbonate	ν_{as} COO^-	[16]
1300–1370	Monodentate carbonate	ν_s COO^-	[16]
1040–1080	Monodentate carbonate	ν C–O	[16]
1530–1620	Bidentate carbonate	ν C=O	[16,22–24]
1250–1270	Bidentate carbonate	ν_{as} COO^-	[16,22–24]
980–1020	Bidentate carbonate	ν_s COO^-	[16,22–24]
1380, 1395, 1600, 2915	HCO_2^-	–	[25]
2570	Chemisorbed H_2S and HS^-	ν S–H	[16]
1620	H_2O	δ H_2O	[16]
1300–1330	Physisorbed SO_2	ν_1	[16,26]
1135–1189	Physisorbed SO_2	ν_3	[16,26]
970, 1050–1065	SO_3^{2-}	–	[16,26,27]
975, 1135–1148	HSO_3^-	–	[16,26,27]
1040, 1350	SO_4^{2-} in $Al_2(SO_4)_3$	–	[27,28]
MgO			
1638–1658	Bicarbonate	ν C=O	[29–31]
1405–1480	Bicarbonate	ν_{as} COO^-	[31]
1217–1220	Bicarbonate	β OH	[29–31]
1040	Bicarbonate	ν_s COO^-	[31]
1506–1560	Monodentate carbonate	ν_{as} COO^-	[29–31]
1385–1421	Monodentate carbonate	ν_s COO^-	[29–31]
1035–1080	Monodentate carbonate	ν C–O	[29–31]
1336	Physisorbed SO_2	ν_1	[32]
1149	Physisorbed SO_2	ν_3	[32]
956, 1040–1080	SO_3^{2-}	–	[27,32]
1300–1050, 1250, 1092	SO_4^{2-} in $MgSO_4$	–	[32]
Mg–Al hydrotalcite			
1650	Bicarbonate	ν C=O	[33]
1480	Bicarbonate	ν_{as} COO^-	[33]
1220	Bicarbonate	β OH	[33]
1510–1560	Monodentate carbonate	ν_{as} COO^-	[33]
1360–1400	Monodentate carbonate	ν_s COO^-	[33]

absorbance at 1611 cm^{-1} has contributions from both HTC and bidentate carbonate, which are the dominant adsorbates at the end of the experiment. The minor peak at 1167 cm^{-1} that is evident after 20 h of adsorption may represent DTC.

3.4. Competitive COS adsorption with propene

To be an effective trapping agent the LDH must remain active in the presence of hydrocarbons. Propene was chosen to represent a typical alkene. Fig. 4 shows the impact of 5% propene on the adsorption of 1% COS at 22 °C. Gas-phase propene has sharp spectral features at 3100, 2960, 1660, 1420, 990, and 910 cm^{-1} which are removed from the spectra after purging. The initial adsorption product consists primarily of bicarbonate (1645, 1408, 1225, and 1090 cm^{-1}), which shifts to both monodentate (1530, 1408, and 1090 cm^{-1}) and bidentate (1607, 1262, and 1011 cm^{-1}) carbonates after approximately 4 h on stream. The sulfur-containing compounds also appear to be present as both HTC (1607 cm^{-1} and a minor shoulder at 1390 cm^{-1}) and DTC (1175, 1090 and 1011 cm^{-1}). While the presence of propene does have an impact on the general shape of the spectra, the end products after 16 h of adsorption are very similar to those observed in the hydrocarbon-free COS adsorption.

3.5. Thermal desorption after H_2S and COS adsorption

After adsorbing H_2S or COS on the samples, they were heated to probe the relative strength of the adsorbate bonds and to attempt to deconvolute the cluster of peaks observed between 1000 and 2000 cm^{-1}. The spectra recorded while cooling down to room temperature after the initial pretreatment at 450 °C were used for the background files during this secondary thermal treatment. Fig. 5a shows the surface transformation of

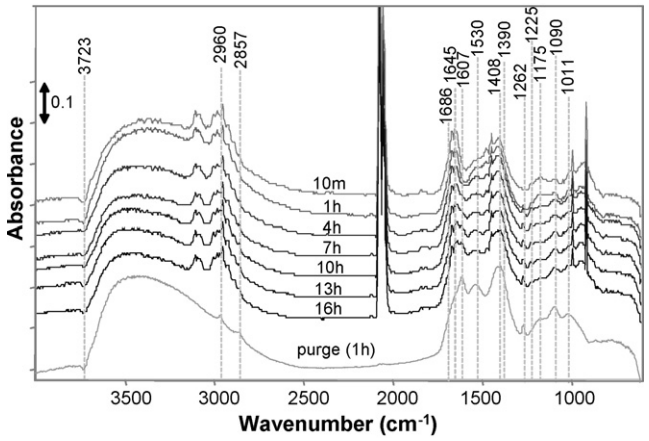

Fig. 4. Background-subtracted DRIFT spectra at 22 °C of $Mg_{0.75}Al_{0.25}$ while flowing 1% COS with 5% propene added. The background spectrum was pretreated $Mg_{0.75}Al_{0.25}$ recorded just prior to introduction of the sulfur-containing stream.

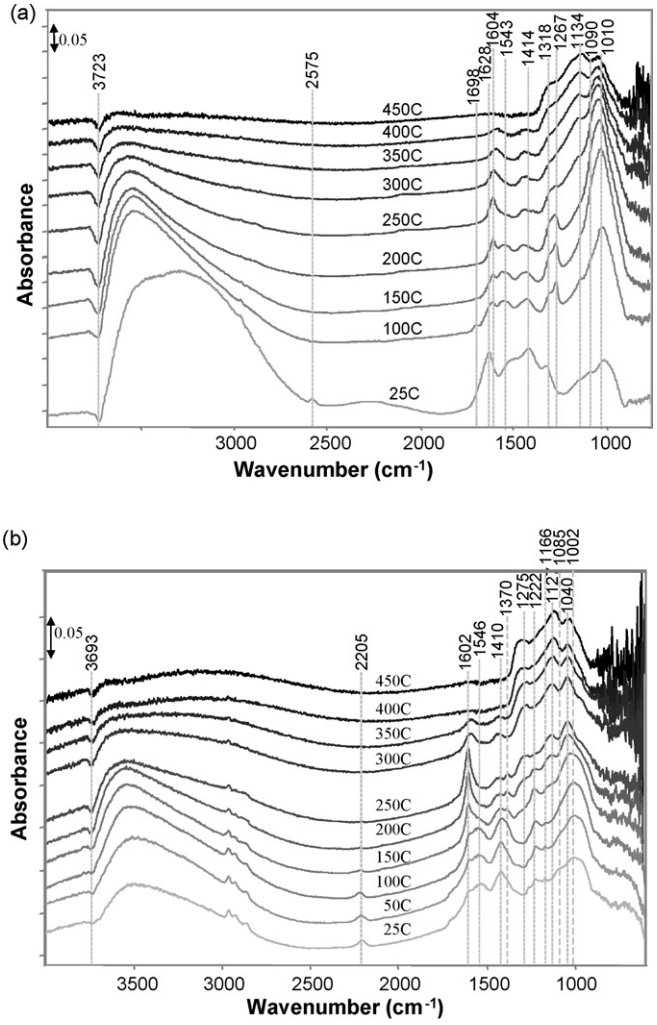

Fig. 5. Background-subtracted DRIFT spectra while heating $Mg_{0.75}Al_{0.25}$ in N_2 to 450 °C after adsorbing (a) 1% H_2S for 16 h, and (b) 225 ppm COS for 65 h. The background spectrum was pretreated $Mg_{0.75}Al_{0.25}$, which was recorded while cooling down from 450 °C during the initial pretreatment.

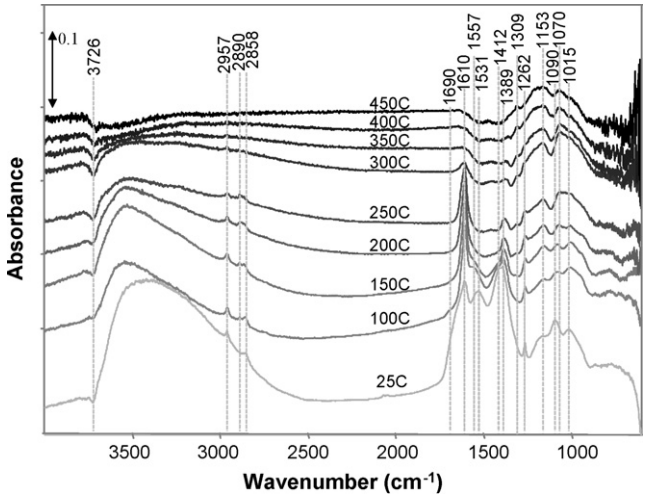

Fig. 6. Background-subtracted DRIFT spectra while heating $Mg_{0.75}Al_{0.25}$ in N_2 to 450 °C after adsorbing 1% COS with 5% propene for 16 h. The background spectrum was pretreated $Mg_{0.75}Al_{0.25}$, which was recorded while cooling down from 450 °C during the initial pretreatment.

$Mg_{0.75}Al_{0.25}$ after adsorbing H_2S for 16 h. The adsorbed water appears to dissipate quickly above 100 °C, which further reinforces this assignment. Beginning at 100 °C, and continuing to 250 °C, peaks at 1604 and 1267 cm^{-1} become more prominent while spectral features between 1100 and 100 cm^{-1} become very large. These observations suggest that upon heating the monodentate carbonate that was observed at 25 °C (resulting from the presence of the CO_2 impurity in the feed) is converted to bidentate carbonate (1604, 1267, 1000–35 cm^{-1}). Simultaneously, SO_3^{2-} (1050–1060 and 970 cm^{-1}), HSO_3^- (1135 and 975 cm^{-1}), and perhaps sulfates (1350 and 1040 cm^{-1}) are forming, and above 400 °C, they dominate the spectra. The oxygen required for the formation of these sulfur species presumably derives from the Mg–Al mixed oxide, although we cannot rule out the possibility that trace oxygen in the feed may have contributed to the formation of these oxidized species.

Fig. 5b shows the spectra recorded during the thermal treatment following COS adsorption. As in the H_2S case, bidentate carbonate (1602, 1275, 1000–35 cm^{-1}) forms between 25 and 250 °C, but here HTC (1602 and 1370 cm^{-1}) is also observed while heating to 250 °C. Above 300 °C, SO_3^{2-}, HSO_3^-, and bulk sulfates dominate the spectra. The final spectrum is very similar to the H_2S case.

Fig. 6 shows the surface transformation of $Mg_{0.75}Al_{0.25}$ after adsorbing 1% COS in the presence of 5% propene for 16 h. The observed trends are nearly identical to the propene-free case, where bidentate carbonate (1610, 1262, 1000–35 cm^{-1}) and HTC (1610 and 1389 cm^{-1}) are evident up to 250 °C and SO_3^{2-}, HSO_3^-, and bulk sulfates dominate the spectra at higher temperatures. Again, the final spectrum in this case is very similar to both the H_2S- and COS-only experiments.

4. Discussion

As shown in Fig. 3a, exposure of calcined hydrotalcite to H_2S results in the formation of a band at 2577 cm^{-1} which can

be assigned to surface SH groups. Concomitantly, spectral changes in the hydroxyl region suggest both the creation of new hydroxyl groups, as well as the consumption of free hydroxyl groups, the latter evidenced by the appearance of a negative band at 3724 cm^{-1}. Similar observations have been reported for H_2S adsorption on a variety of oxides [16,17], for which it was suggested that adsorption proceeds via H_2S dissociation, e.g.:

$$H_2S + M{-}O{-}M \rightarrow M{-}SH + M{-}OH \quad (2)$$

Another adsorption route that seems particularly plausible on mixed oxides is through the interaction of H_2S with a defective site, or oxygen vacancy, resulting in incorporation of S^{2-} in the lattice. As detailed by Davydov et al. for Al_2O_3 [16], this involves the consumption of a hydroxyl group and the formation of molecularly adsorbed H_2O (as well as a new hydroxyl group), which fits well with the spectroscopic data:

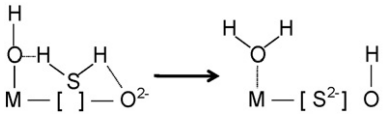

(3)

$$(H_2S)_{ads} + [\,] + M^{n+}O^{2-} + OH^- \rightarrow (H_2O)_{ads} + OH^- + M^{n+}S^{2-} \quad (4)$$

Additionally, in the case of MgO, its high basicity makes it probable that S^{2-} can be incorporated directly into the surface [16], i.e.:

$$Mg{-}O{-}Mg + H_2S \rightarrow Mg{-}S{-}Mg + H_2O \quad (5)$$

In the case of COS adsorption, the total absence of identifiable sulfur species at short reaction times suggests a similar incorporation of S^{2-}. Indeed, Haag and Miale found that the surface of MgO underwent sulfidation when exposed to COS at 811 K (contact times being on the order of seconds) [34]:

$$MgO + COS \rightarrow MgS + CO_2 \quad (6)$$

A thiocarbonate intermediate was proposed for this reaction [34], although our DRIFTS data are unable to provide evidence of such an intermediate. The CO_2 produced is evidently adsorbed on the surface, giving rise to the observed bicarbonate together with either monodentate and/or bidentate carbonate. At longer reaction times two types of sulfur-containing species are observable, corresponding to HTC and DTC. The fact that growth of the HTC band is simultaneous with a decrease in the intensity of the bicarbonate bands suggests that the HTC is derived from the bicarbonate. Lavalley et al. have reported that when H_2S is adsorbed on CO_2-treated γ-alumina, the carbonate bands are weakened and new bands appear at 1570 and 1340 cm^{-1} which can be assigned to HTC [17]:

$$Al{-}O(CO)OH + H_2S \rightarrow Al{-}O(CO)SH + H_2O \quad (7)$$

The origin of the required H_2S is unclear, although it may be derived from the hydrolysis of M–SH (M = Mg or Al) or lattice S^{2-} species (i.e., the reverse of reactions (2) and (4)) by adventitious water.

At long reaction times DTC is also observed. Lavalley and co-workers [21] have established that this is formed upon adsorption of CS_2 onto basic O^{2-} sites in metal oxides:

$$M{-}O{-}M + CS_2 \rightarrow M{-}SC(S)O{-}M \quad (8)$$

The presence of CS_2 can in turn be rationalized based on the ability of COS to undergo disproportionation:

$$2COS \leftrightharpoons CS_2 + CO_2 \quad (9)$$

Haag and Miale [34] showed that metal oxides are able to catalyze this reaction, MgO being a particularly efficient catalyst; at 538 °C, 90% attainment of equilibrium was observed at a contact time of 0.2 s. Although the equilibrium constant for this reaction is very small at room temperature (2.4×10^{-3} based on the reported value of ΔG° [34]), removal of the CS_2 and CO_2 products by adsorption may enable non-equilibrium surface concentrations of CS_2 to accumulate.

Overall, the mechanism of COS adsorption on calcined hydrotalcite is rather different to that observed for less basic oxides (such as Al_2O_3, ZrO_2 and TiO_2). For the latter, it is well established that COS adsorption occurs primarily via the formation of HTC species (the primary product), which can undergo hydrolysis to afford CO_2 and H_2S which are in turn adsorbed [35,36]. In the case of calcined hydrotalcite, the strongly basic surface reacts with COS to generate S^{2-} species and CO_2, the latter being adsorbed mainly in the form of bicarbonate.

5. Conclusions

Both $Mg_{0.65}Al_{0.35}$ and $Mg_{0.75}Al_{0.25}$ demonstrated the ability to adsorb significant concentrations of H_2S and COS at 25 °C. The adsorption of H_2S proceeds via the substitution of lattice oxygen with sulfur which results in the formation of H_2O on the surface of the calcined LDH. COS adsorption is more complicated, although it appears that a similar substitution of lattice oxygen with sulfur is taking place. This results in the formation of CO_2 and subsequently bicarbonates and carbonates. The formation of hydrogen thiocarbonate is also involved, although this form is generally only observed in the later stages of adsorption and appears to form at the expense of bicarbonate. The $Mg_{0.75}Al_{0.25}$ LDH retained its ability to adsorb COS in the presence of propene.

Acknowledgements

The authors thank Dr. Louis Powell of the Oak Ridge Y-12 National Security Complex for use of the FTIR spectrometer and DRIFTS accessory. This research was sponsored by the State Partnership Program at Oak Ridge National Laboratory, which is managed by UT-Battelle, LLC, under US Department of Energy contract number DE-AC05-00OR 22725.

References

[1] R. Farrauto, S. Hwang, L. Shore, W. Ruettinger, J. Lampert, T. Giroux, Y. Liu, O. Ilinich, Annu. Rev. Mater. Res. 33 (2003) 1.
[2] F. Cavani, F. Trifiró, A. Vaccari, Catal. Today 11 (1991) 173.
[3] Z. Yong, A.E. Rodrigues, Energy Convers. Manage. 43 (2002) 1865.
[4] T. Yamamoto, T. Kodama, N. Hasegawa, M. Tsuji, Y. Tamaura, Energy Convers. Manage. 36 (1995) 637.
[5] M. Tsuji, G. Mao, T. Yoshida, Y. Tamaura, J. Mater. Res. 8 (1993) 1137.
[6] A.E. Palomares, J.M. López-Nieto, F.J. Lázaro, A. López, A. Corma, Appl. Catal. B 20 (1999) 257.
[7] A. Corma, A.E. Palomares, F. Rey, F. Márquez, J. Catal. 170 (1997) 140.
[8] E.W. Albers, H.W. Burkhead Jr., US 5,928,496 (1999).
[9] T.J. Pinnavaia, J. Amarasekera, US 5,358,701 (1994).
[10] D.E. Sparks, T. Morgan, P.M. Patterson, S.A. Tackett, E. Morris, M. Crocker, T.J. Toops, Appl. Catal. B 82 (2008) 190–198.
[11] W.T. Reichle, J. Catal. 94 (1985) 547.
[12] T.J. Toops, D.B. Smith, W.P. Partridge, Appl. Catal. B 58 (2005) 245.
[13] G.L. Powell, M. Milosevic, J. Lucania, N.J. Harrick, Appl. Spectrosc. 46 (1992) 111.
[14] W.T. Reichle, S.Y. Kang, D.S. Everhardt, J. Catal. 101 (1986) 352.
[15] F. Rey, V. Fornes, J.M. Rojo, J. Chem. Soc., Faraday Trans. 88 (1992) 2233.
[16] A.A. Davydov, in: C.H. Rochester (Ed.), Infrared Spectroscopy of Adsorbed Species on the Surface of Transition Metal Oxides, John Wiley & Sons, Chichester, England, 1990.
[17] J.C. Lavalley, J. Travert, T. Chevreau, J. Lamotte, O. Saur, J. Chem. Soc., Chem. Commun. (1979) 146.
[18] E. Laperdrix, I. Justin, G. Costentin, O. Saur, J.C. Lavalley, A. Aboulayt, J.L. Ray, C. Nedez, Appl. Catal. B 17 (1998) 167.
[19] J.C. Lavalley, Catal. Today 27 (1996) 377.
[20] C. Rhodes, S.A. Riddel, J. West, B.P. Williams, G.J. Hutchings, Catal. Today 59 (2000) 443.
[21] A. Sahibed-Dine, A. Aboulyat, M. Bensitel, A.B.M. Saad, M. Daturi, J.C. Lavalley, J. Mol. Catal. A 162 (2000) 125.
[22] C. Morterra, C. Emanuel, G. Cerrato, G. Magnacca, J. Chem. Soc., Faraday Trans. 173 (1977) 1544.
[23] M. Kantschewa, E.V. Albano, G. Ertl, H. Knözinger, Appl. Catal. 8 (1983) 71.
[24] P. Chaumette, P. Courly, J. Barbier, T. Fortin, J.C. Lavalley, C. Chauvin, A. Kiennemann, H. Idriss, R.P.A. Sneeden, B. Denise, in: Proceedings of the 9th International Congress on Catalysis, vol. 2, Chem. Inst. Can., Ottawa, 1988, p. 585.
[25] A. Iordan, M.I. Zakiz, C. Kappenstein, Phys. Chem. Chem. Phys. 6 (2004) 2502.
[26] A. Datta, R.G. Cavell, R.W. Tower, Z.M. George, J. Phys. Chem. 89 (1985) 443.
[27] X. Zhang, G. Zhuang, J. Chen, Y. Wang, X. Wang, Z. An, P. Zhang, J. Phys. Chem. 110 (2006) 12588.
[28] Ch. Sedlmair, K. Seshan, A. Jentys, J.A. Lercher, Catal. Today 75 (2002) 413.
[29] V.A. Ivanov, A. Piéplu, J.C. Lavalley, P. Nortier, Appl. Catal. A 131 (1995) 323.
[30] R. Philipp, K. Fujimoto, J. Phys. Chem. 96 (1992) 9035.
[31] J.V. Stark, D.G. Park, I. Lagadic, K.J. Klabunde, Chem. Mater. 8 (1996) 1904.
[32] A.J. Goodsel, M.J.D. Low, N. Takezawa, Environ. Sci. Technol. 6 (3) (1972) 369.
[33] J.I. Di Cosimo, V.K. Diez, M. Xu, E. Iglesia, C.R. Apesteguia, J. Catal. 178 (1998) 499.
[34] W.O. Haag, J.M. Miale, in: Proceedings of the 6th International Congress on Catalysis, London, Vol. 1, 1976, p. 397.
[35] P.E. Hoggan, A. Aboulayt, A. Pieplu, P. Nortier, J.C. Lavalley, J. Catal. 149 (1994) 300.
[36] J. Bachelier, A. Aboulayt, J.C. Lavalley, O. Legendre, F. Luck, Catal. Today 17 (1993) 55.